

# DESIGN AND ANALYSIS OF A TRANSONIC FLUTTER RESEARCH COMPRESSOR

Hans E. Mårtensson<sup>1</sup>, Jan Östlund<sup>1</sup>, Ronnie Bladh<sup>2</sup>, Björn Grüber<sup>3</sup>

<sup>1</sup> VOLVO Aero Corporation  
Trollhättan, Sweden  
e-mail: [hans.martensson@volvo.com](mailto:hans.martensson@volvo.com)

<sup>2</sup> Siemens Industrial Turbomachinery AB  
Finspong, Sweden  
e-mail: [ronnie.bladh@siemens.com](mailto:ronnie.bladh@siemens.com)

<sup>3</sup> MTU Aero Engines  
München, Germany  
e-mail: [bjoern.grueber@mtu.de](mailto:bjoern.grueber@mtu.de)

**Keywords:** flutter, simulation, CFD, compressor, transonic, mistuning.

**Abstract:** The design and analysis by modern CFD based methods is described. Flutter in jet engine and gas turbine compressors is one of the major problems facing the blade designer. Methods development is continually delivering improved methods that allow the inclusion of new physics. In particular with new and advanced methods the need grows for experimental validation that is adapted for the method. In the European framework program the FUTURE project is dedicated to flutter, and as part of this one work package addresses the objective of validation on a transonic research compressor.

The compressor blades are aerodynamically designed to fit within the specific rig capacity with respect to power, speed and torque. In the design one goal is to obtain a free flutter condition in the rig in a controlled manner. This is opposite to the normal design goal, where the analysis is used to prove that a design cannot flutter. The design target from the outset is to have a 1st flex forward travelling mode fluttering at a low nodal diameter. The test vehicle design includes variable inlet guide vanes to facilitate control of parameters affecting the flutter limits at the test, such as relative Mach number and incidence. In addition to testing for the free flutter limit the test includes an excitation system that allows the determination of system damping at any point in the operating envelope.

Three different CFD tools at three companies are used supporting the design work for determining the aerodynamic damping inside the operating envelope. A quantitative comparison reveals that the predicted aerodynamic damping characteristics vary significantly between the employed numerical tools, thus underlining the need for validation and extensive test data. Computation of the aerodynamic damping is made along the compressor speed lines revealing both continuous variations of the aerodynamic damping as well as rapid changes, “flutter bites”, where the damping drops off rapidly. Effects of mistuning are also evaluated, as this is expected to affect the results of the testing.

## **1 INTRODUCTION**

Flutter in jet engine and gas turbine compressors is one of the major problems facing the blade designer. A research program, FUTURE, in the European 7<sup>th</sup> framework is in progress with the goal to address research into the phenomenon. FUTURE brings together European well-reputed centers-of-excellence in order to reach major scientific and technical objectives in striving towards flutter-free turbomachine blades. By advancing the state-of-the-art in flutter prediction capabilities and design rules, the FUTURE project will lead to benefits in terms of decreased development cost, reduced weight and fuel consumption, and increased ability to efficiently manage flutter problems occurring on engines in service. Eight interconnected turbine and compressor experiments will be performed in the project, in combination with numerical modeling of vibrating blades and the related unsteady aerodynamics. A major part of the research in the FUTURE program directed towards compressors is based on developing an experiment allowing relevant and controlled studies of flutter in a transonic compressor. The compressor rotor is designed for this project collaboratively between 3 companies, VAC (VOLVO Aero Corporation) is the work package leader and designs the blade, SIT (Siemens Industrial Turbomachinery) and MTU (MTU Aero Engines) makes design supporting flutter predictions. Other partners in the program contribute to the research with large range of advanced analyses and tests.

Flutter in the compressor is a condition resulting from arriving at an operating point where the aerodynamic damping becomes negative and larger than the damping inherent in the structure. As the condition is reached the blades vibrates with increasing amplitude, either ending in a limit cycle oscillation (LCO) or increasing exponentially in amplitude to failure. For designs where the blades and the disk are made from a single piece of material (BLISK) the structural damping is extremely low. For practical purposes in design a negative aerodynamic damping is often considered as the flutter limit.

The goal of the experiment at hand is to operate the compressor in both free flutter and to measure aerodynamic damping at widely varying operating conditions. Variability in terms of operating conditions is increased by the introduction of a variable inlet guide vane. The free flutter condition is particular in the test context in the sense that the risk must be considered that a blade fails rapidly. A loss of test objectives and expensive hardware is the likely outcome of such an event.

Firstly the blade is designed together with instrumentation directly for the experiment, which is described in detail below. A second necessary component of the experimental design is an excitation system to provide a controlled excitation of the blade. The use of an excitation system allows the characterization of the aerodynamic damping at multiple operating points, which increases drastically the possibilities for validating CFD methods and the understanding of aerodynamic damping. The flutter limit can also be approached in the test observing the drop in system damping as it approaches zero, i.e. the flutter limit.

## **2 DESIGN OF THE COMPRESSOR STAGE FOR THE TEST**

Design of a compressor blade is always a complex task that needs to consider many requirements and needs simultaneously. An important goal for this design is to study free flutter which means that the design should allow that flutter occurs inside the compressor envelope. Normally flutter is a condition that the designer tries very hard to avoid.

A first task is to select a performance operating point that is representative for modern compressors and that is also adapted to the rig limitations. The rig limitations in table 1 are given by the drive system in terms of shaft power, torque and allowable operating speed.

Maximum power	800 kW
Maximum torque	340 Nm
Maximum shaft speed	20,300 rpm
Tip Diameter	380 mm

Table 1: Rig operating parameters

Further the rig is to be fitted with an inlet frame and a variable guide vane system that allows control of the inlet swirl. Much of the existing hardware is re-used, i.e. shaft components, bearing system, stator and the entire rig downstream of the stator [1]. Figure 1 shows a cross section of the rig test section with the test object, without excitation system.

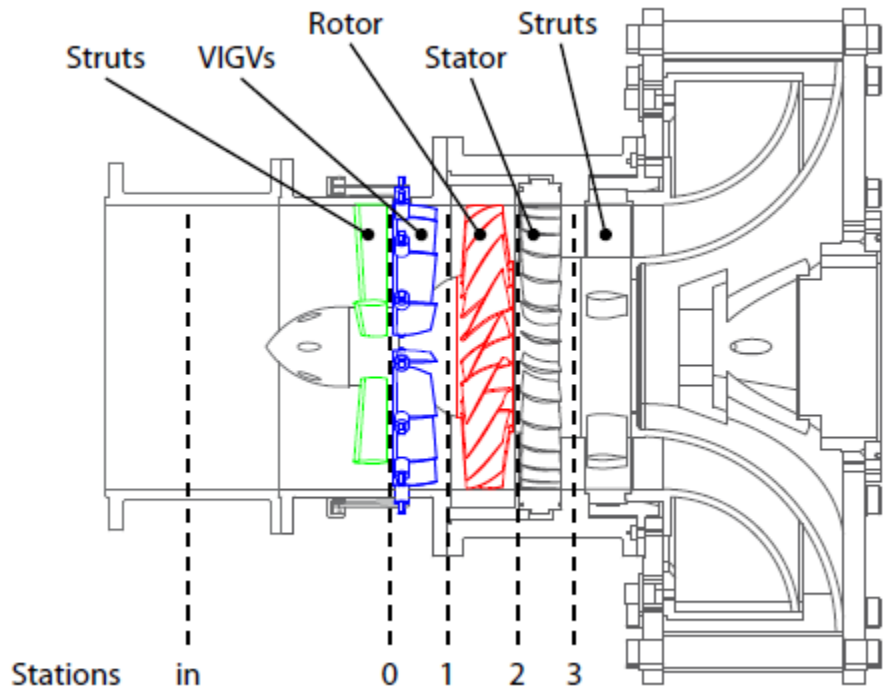


Figure 1: Cross section of rig with test compressor

Within the rig constraints an aerodynamic design point (ADP) was selected at 18,000 rpm with a pressure ratio of 1.42 and a mass flow of 13.8 kg/s. The choice of operating point inside the rig limits provides the possibility of running the rig at a wide range of off-design operating points, both above and below the design point.

A variable inlet guide vane is incorporated in the design of the test vehicle so that the inlet flow angles can be varied over a range of 30 degrees. The profiles are of a simple conception, with no turning at design point, but allow testing at substantial changes in incidence, mass flows and pressure ratios for a given shaft speed.

A computed compressor performance map for nominal VIGV setting is shown in figure 2. This is derived using CFD at zero tip clearance, thus a slightly lower mass flow, efficiency

and pressure ratio can be expected in test. In terms of radial profile the pressure and temperature rise is larger at the tip. Two factors govern the radial work profile, firstly the stator was not subject to re-design and the incidence could not be allowed to increase too much at design point. Secondly, with the understanding that the tip is the more sensitive part with respect to flutter, particularly for the 1F (1<sup>st</sup> flexural) mode, using the available rig power in the tip region was prioritized.

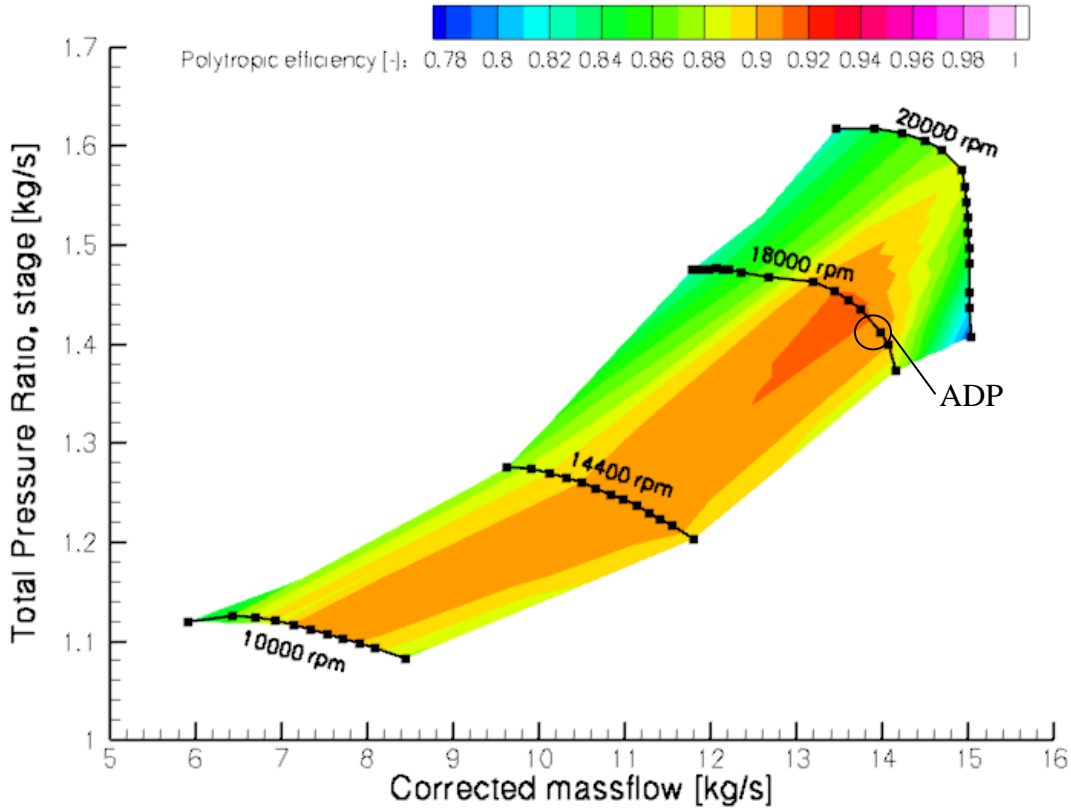


Figure 2: Compressor map for fixed nominal guide vane setting from design analysis

Early design loops showed that it would be difficult to ensure that the blade flutters within the constraints of the design space. Design measures were therefore employed to increase the blade sensitivity to flutter. Decreasing the tip chord results in an increased suction side Mach number at ADP, while reducing the capability for maximum pressure rise, or stall margin. Also the reduced chord leads to a reduction in reduced frequency, which is a commonly used parameter for flutter sensitivity. The selection of the blade leading edge angle is such that the stagnation point is centered at the leading edge of the blade at ADP. Figure 3 shows the resulting blade-to-blade pressure distribution at 90 % span. The aerodynamic loading is generally high in the outer portion of the blade, as the intent is to work with high loading in the region that will affect the 1F mode stall flutter. An added benefit of this is that the root sections can be designed with low camber which decreases the profile stiffness, and thus reduces the frequency of the 1F mode. Whereas a thickness reduction at the root increases the blade stresses thus reducing the strength, the reduction in camber has no impact on root mean stress.

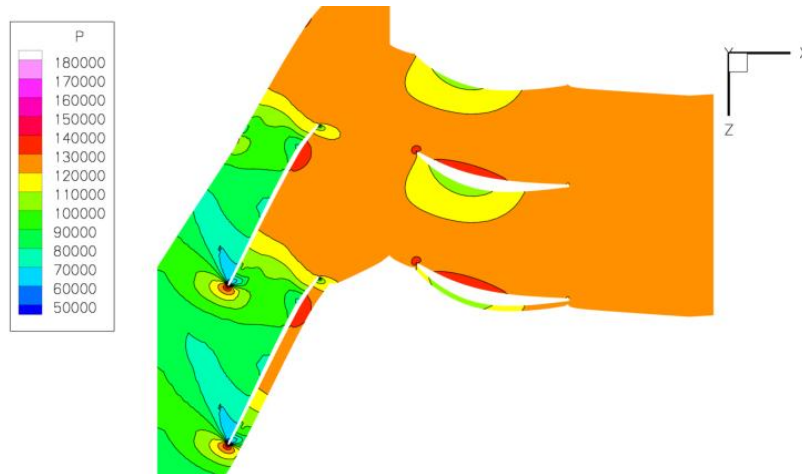


Figure 3: Blade-to-blade pressure distribution at the tip, unit is Pa

The thickness of the blade must be sufficient to allow for pressure probes to be embedded in the blade. A second condition is on blade stress, since the direct intent is to operate in flutter where the alternating stress must be expected to become high. A relatively low mean stress in the blade is therefore necessary to allow vibration without exceeding the HCF (High Cycle Fatigue) limits. At the maximum shaft speed the tip speed of the blade is 403 m/s. The tip thickness chosen is 2.4% of the tip chord. A thicker tip would be beneficial with respect to lowering the blade 1F frequency, but the negative consequence is that the heavier tip increases blade stresses in the lower parts of the blade imposing limitations on instrumentation. Figure 4 shows the blade profiles of the selected design together with a side view of the tangential displacements of the first flex mode.

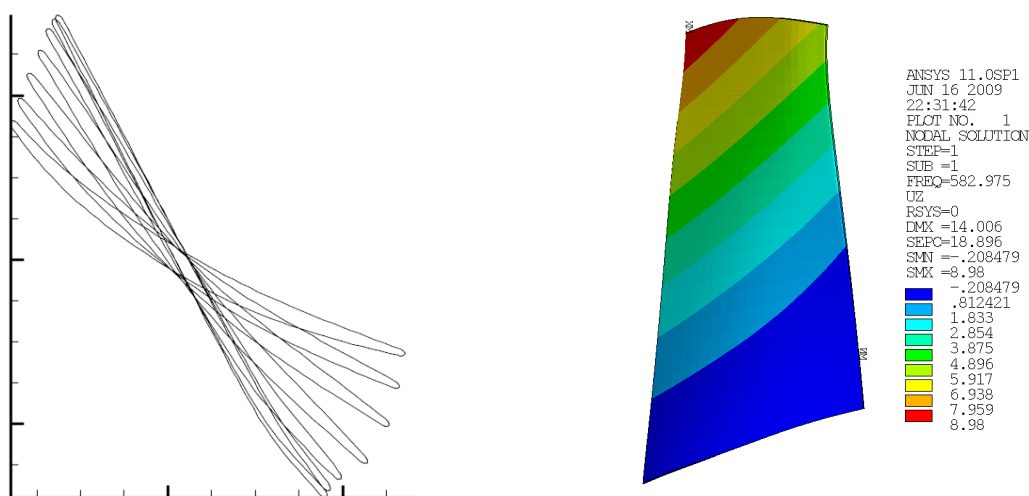


Figure 4: Profile stack (left) and displacements of the 1<sup>st</sup> flex mode (right)

Apart from the chord and loading also the mode shape affects the tendencies towards flutter. In the present blade design the max thickness and camber are located far back along the chord, which promotes larger torsion content in the 1F mode. The computed frequency of the 1F mode at ADP is  $f = 583\text{Hz}$  from a modal analysis of the blade fixed at the root in the VAC analysis using ANSYS. Together with the relative velocity and chord,  $c$ , at 90% chord

this gives a reduced frequency,  $k = \frac{\pi \cdot c \cdot f}{V_{rel}} = 0.32$  at ADP for the first flex mode:

As a comparison of the modal analysis MTU in this case used the open source FEM-solver calculix [2]. The computed frequency is  $f=584.5$  Hz at 18,000 rpm, which is for all practical purposes the same result as in the VAC case.

### 3 COMPARISON OF AERODYNAMIC ANALYSIS

All aerodynamic damping analyses are here made using harmonic perturbations of a steady state flow. It is therefore interesting to compare the steady state results in some detail since this will affect also the aerodynamic damping result. The design iterations are made using the VAC code VolSol [3] without tip clearance on a standardized coarse mesh. The compressor map in figure 2 was based on this code and thus this will be used as a reference for comparison. MTU and SIT codes have been used for the same analyses supporting the design work. The computations performed by SIT employ the in-house CFD code TF3D, which solves the unsteady 3D compressible full Navier-Stokes equation with a Baldwin-Lomax turbulence model [4] on a simple H grid. The details of the TF3D solver are not disclosed here, but can be found in [5–7]. For the MTU steady-state flow analyses the TRACE code [8,9] developed at DLR is used. The compressible Reynolds-averaged 3D Navier-Stokes equations with a  $k-\omega$  turbulence model are solved on block structured meshes. The unsteady aerodynamic forces due to the blade motion are obtained by the time linearized Euler method Lin3d developed by Kahl [10-12]. Table 2 compiles the more important properties that differ among the codes.

	VAC	SIT	MTU
Code used	VolSol	TF3D	TRACE+Lin3d
Tip clearance	No	0.5 mm	0.5 mm
Turbulence model	$k-\epsilon$ , wall function	Baldwin-Lomax	$k-\omega$ , wall function

Table 2 Codes used in the study

A standard way of presenting the key performance numbers of compressors is to use a speed line plot. Here the speed is held constant and the back pressure is increased in steps so that the aerodynamic load increases until the simulation is no longer stable. Figure 5 shows the pressure ratio over the stage from rotor inlet to stator outlet vs. mass flow. The VAC code has a higher choke mass flow than the MTU and SIT calculations which is most likely due to the absence of tip clearance in this model.

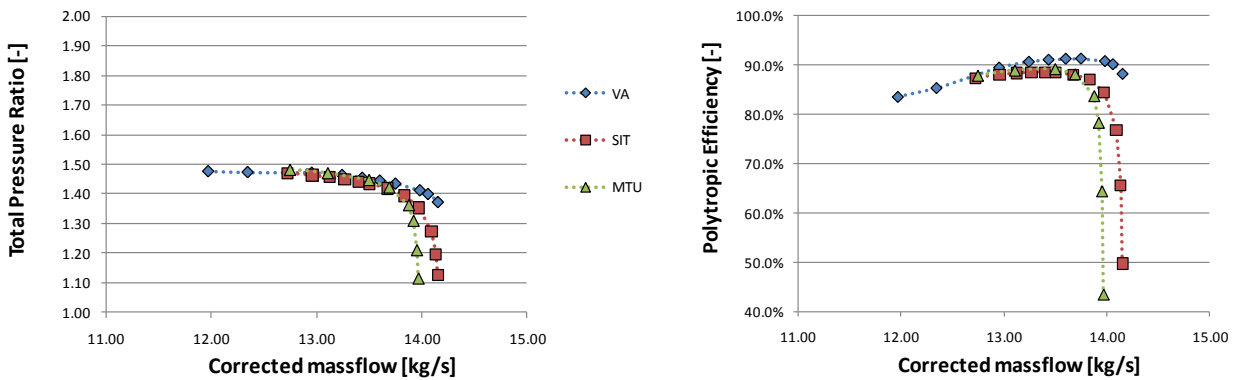


Figure 5 Speed line comparisons for the different steady state computations

Other differences that may affect this include also the turbulence model since blockages might differ. The difference from highest choke flow (VAC) and lowest (MTU) is approximately 2% which is a reasonable variation. The speed lines are in good agreement above the design point where the mass flow starts to decrease. The VAC simulation allows a lower mass flow before the simulations diverge. This can be an effect of the absence of tip leakage or an effect of how the solvers are affected by the separations that start appearing in the stator and grows as the flow rate is decreased. The differences in aerodynamic performance are considered as normal and not revealing any discrepancies.

For all simulations of the mean flow the complete stage is computed. In some more detail the Mach numbers in the blade-to-blade planes are compared in figure 6 in the rotor approximately at the same operating point, i.e. near the ADP pressure ratio 1.42 at 18000 rpm.

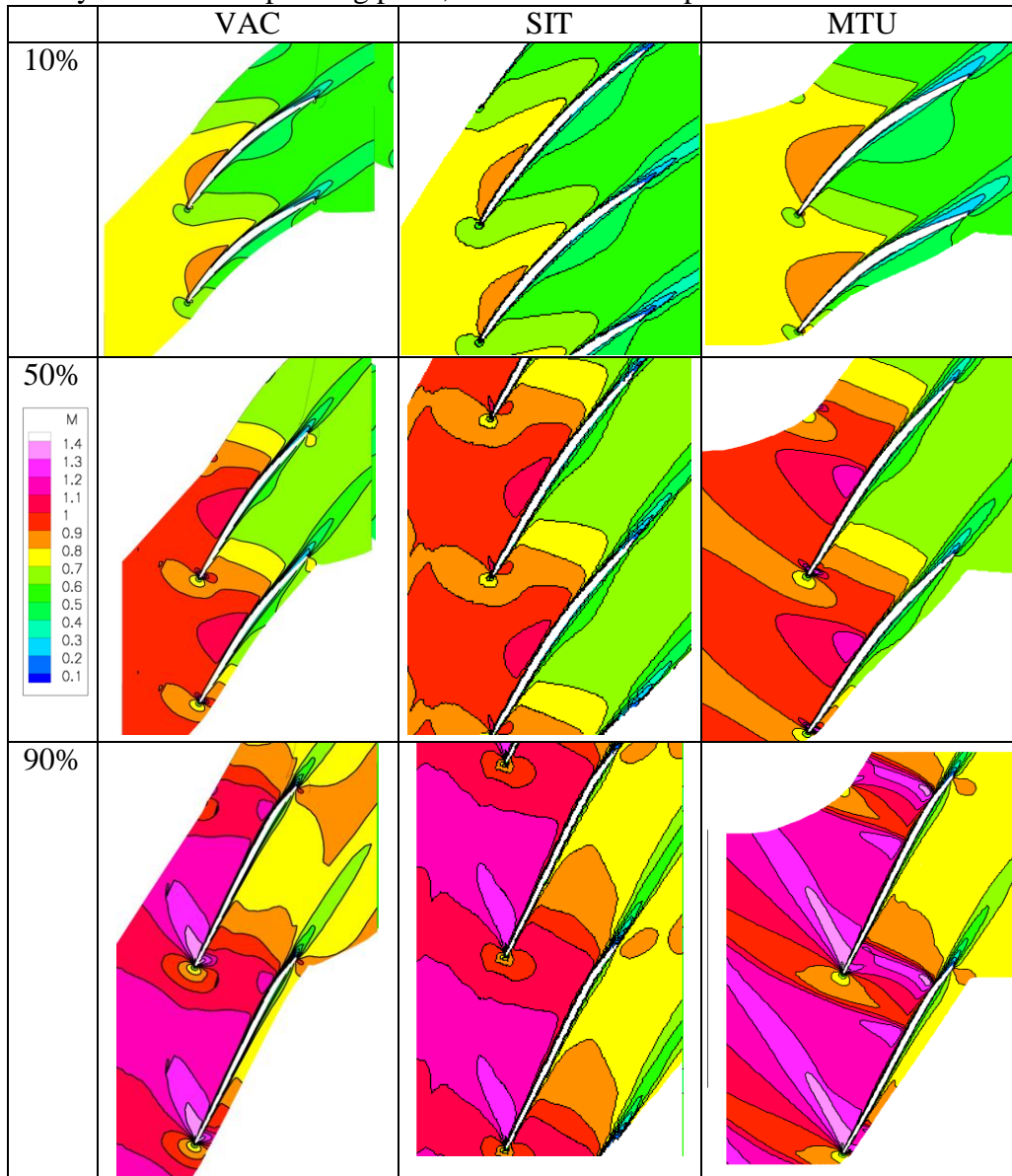


Figure 6: Comparison of Mach numbers at 10%, 50% and 90% span near ADP for the codes used in the study

The Mach number plots confirm that differences are present but modest in the performance calculation in general.

## 4 FLUTTER ANALYSIS OVER THE OPERATING ENVELOPE

In the test the compressor will be run in a large envelope. The basic aerodynamic damping of the lowest damped mode in the VAC design analysis is therefore computed at 3 speeds and plotted into the compressor map in figure 7. The aerodynamic damping analysis for this is conducted using a linearized harmonic Euler analysis [3,13] for the rotor alone on a mesh without tip clearance. Mode shape and frequency are obtained from a modal analysis using a blade fixed to ground.

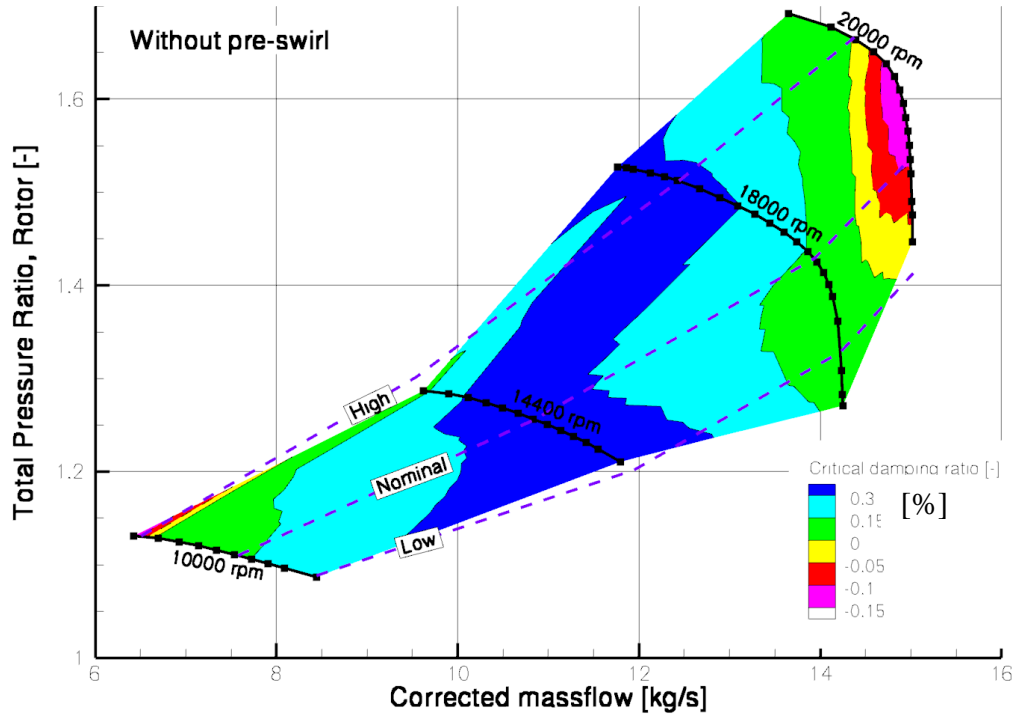


Figure 7: Minimum computed damping mapped into the compressor map

The aerodynamic damping map shows two distinct areas where the aerodynamic damping is negative and thus where flutter is most likely to occur: at 20,000 rpm over a large pressure ratio range and at 10,000 rpm just at the stall line. Finding a flutter region at the high speed end of the compressor map is expected as the reduced frequencies fall with increasing mass flows and the relative Mach number increases. In the second region at 10,000 rpm the tip speed is 200 m/s and the relative flow velocities subsonic, but at the high incidence angles supersonic pockets may still be found. At the higher speeds the aerodynamic damping stays positive in the analysis as the stall line is approached. It must be noted here that particularly the computation at or near the stall line includes several difficulties. Computing the steady state flow when the flow starts to separate at the tip is a challenge in itself involving complex flow physics. It is further complicated by the unsteady interactions that may or may not occur in reality as the flow condition approaches its stability limit, such as rotating stall. The computation of aerodynamic damping in this region should therefore be taken with particular care. Sharp drops in stability are exhibited in several of the analyses as the “numerical stall”, limit is approached, i.e. the maximum attained pressure ratio along the speed line. For the continued research work these will be of particular interest in terms of understanding the physics and how it should be modeled.

#### 4.1 Results and comparison of different aeroelastic computations

All computations performed in this study make use of the energy method that was developed by Carta [14]. It assumes that the effect of aerodynamic forces on the structural dynamic properties of the aeroelastic system can be neglected, i.e. there will be no changes of mode shapes and frequencies due to unsteady aerodynamic blade loadings. Hence the unsteady aerodynamic forces, mode shapes and frequencies can be calculated independently.

One interesting way of starting to compare the results of the different analyses is to study the minimum damping while increasing the back pressure at constant speed. This allows the evaluation of the effects of the aerodynamic loading on the aerodynamic damping. In figure 8 the aerodynamic damping is evaluated at several speeds using the different codes. 18,000 rpm and 20,000 rpm are analyzed using all three codes for back-to-back comparison. The minimum damping is systematically larger in the MTU analysis, but a general trend of a lower minimum damping at the higher speed is clear in the analyses. The aerodynamic damping generally appears to be increasing with pressure ratio at these speeds above the operating line, until a more or less sharp drop may occur near the end of the speed line. In some analyses this drop occurs and in some it does not. While difficult to conclude on, it may be the case that the drop in damping will always occur near stall, but whether it will be observed or not depends on if the mean flow solution breaks down before it is noticeable. In some of the analyses the damping also rises towards the choke side so that a minimum forms as already observed also in figure 7. The speed line made for a -15 degrees inlet flow angle shows that also at constant shaft speed the increased loading and mass flow has a similar effect in decreasing the damping levels. The use of the variable inlet guide vane (VIGV) is thereby useful as another independent variable that can be used to modify the aerodynamics and control the susceptibility to flutter.

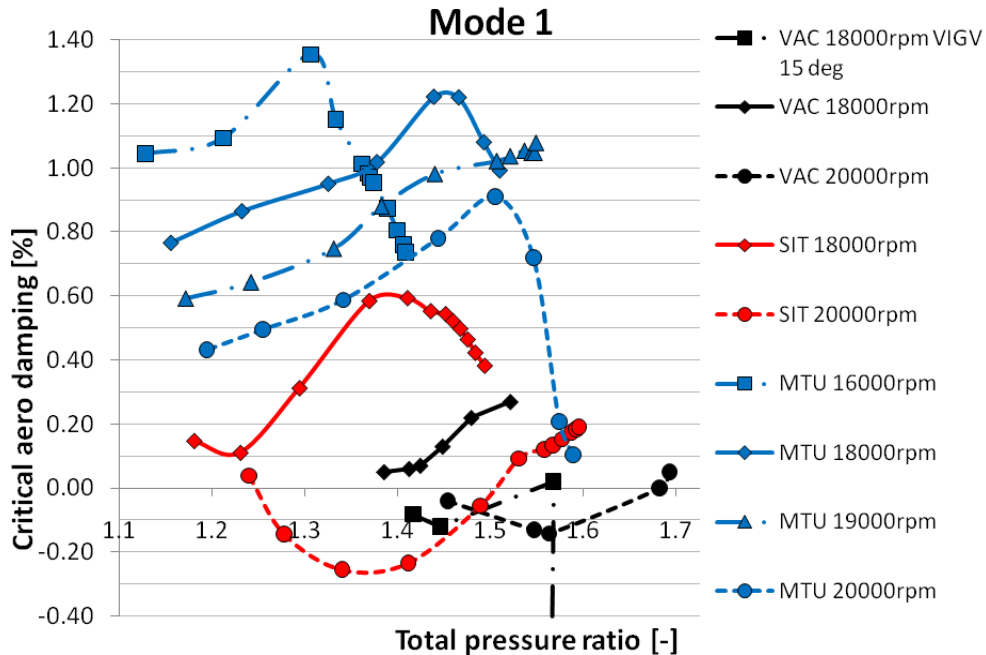


Figure 8: Minimum aerodynamic damping vs. pressure ratio over rotor for first flex mode.

The aerodynamic damping varies strongly with the nodal diameter (ND) of the mode. Figure 9 shows a plot of the variation of the aerodynamic with nodal diameter for computations using three codes near the ADP. While the general shape is the same in all three cases some details

differ. While all three show minima in aerodynamic damping at the lower forward travelling mode the level is different with the VAC calculation at 0.1% and the MTU calculation at approximately 1%, while the levels in general are much more similar. The comparison of the minimum value this way points out a very important fact about the minimum damping calculation in that it is made up from the difference between large numbers. The MTU calculation also has local a minimum at  $-2ND$ , which the other two cases do not exhibit.

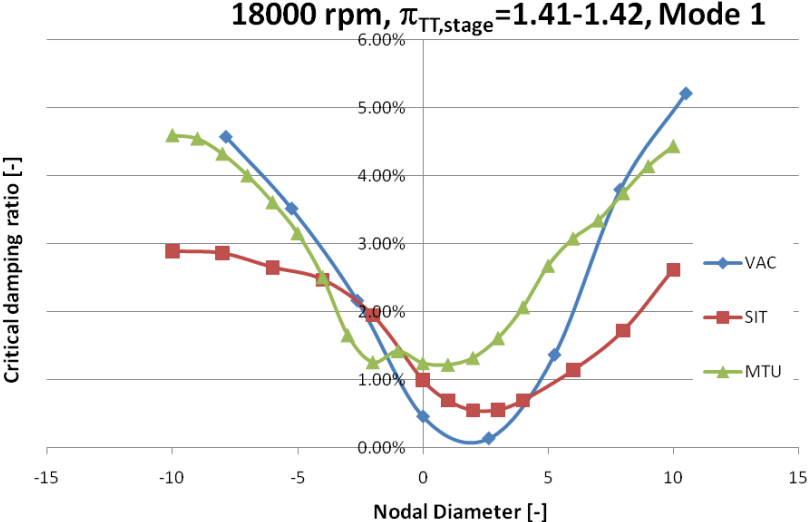


Figure 9: Critical aero dynamical damping ratio vs. nodal diameter at  $\prod_{TT} = 1.41$  and 18,000 rpm.

In figure 10 again the results are qualitatively very similar. Quantitatively the minimum damping also becomes very similar in the sense that the variation between the codes is less than 0.2%. However, again highlighting the difficulty of predicting the flutter limit, the VAC calculation is in this case on the negative side, while the MTU and SIT calculations stay on the positive side of zero. A straight on/off view with respect to flutter would give very different results in this case. One analysis indicates flutter and the others not, while in reality the results may be fairly similar. Again the results consistently indicate the lower forward travelling nodal diameters as the critical ones.

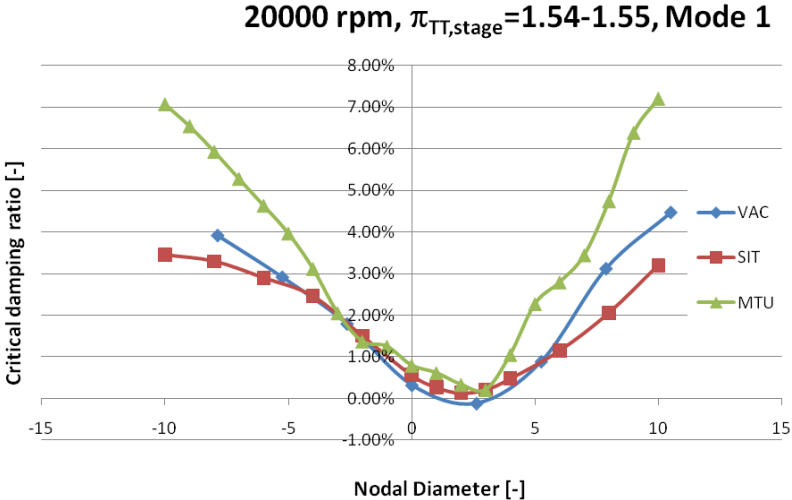


Figure 10: Critical aero dynamical damping ratio vs. nodal diameter at  $\prod_{TT} = 1.54$  and 20,000 rpm.

Note that differences in steady state solution in terms of mass flow, due to for instance tip clearance effects at a given pressure ratio, will affect the comparisons in figures 9 and 10. Analyzing the details of how the aerodynamic work is formed by looking at the distribution over the surface is revealing to the problem of predicting flutter. Here an example is provided using the MTU analysis for an operating point with transonic flow in the tip region of the blade. A detailed investigation of the flow phenomena indicates that the shocks on the pressure and suction side of the rotor are the main contributors to the local aerodynamic excitation and damping and hence responsible for flutter. Figure 11 clearly shows that only the tip region of the blade contributes significantly to the aerodynamic work of the entire rotor.

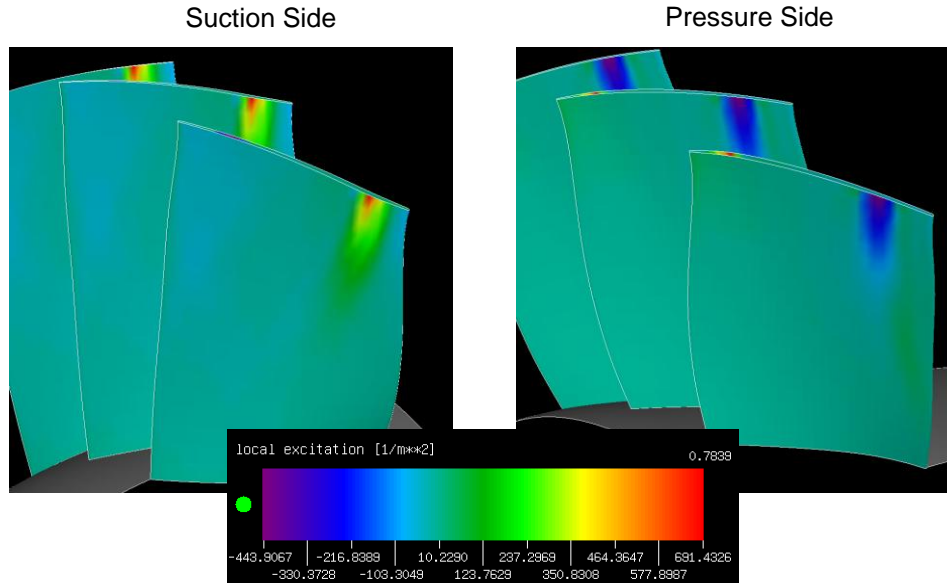


Figure 11: Normalized local aerodynamic excitation distribution,  
(rpm 20,000, IBPA= -34.3°, ND= +2; near stall)

In Figure 12 the local aerodynamic excitation along the axial position for a tip section is plotted. The diagram shows that the shock on the suction side (green line) excites the blade whereas the shock on the pressure side (red line) damps it. The sign of the sum of both curves decides if the blade is excited or damped. Small deviations in the prediction of the shocks could change the flutter result significantly.

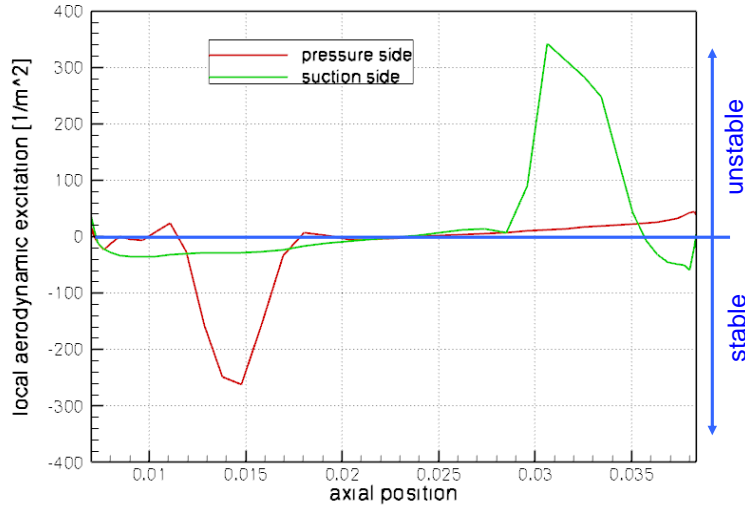


Figure 12: Normalized local aerodynamic excitation distribution

Apart from showing the regions where the aerodynamic damping is most affected, figure 12 also points to one severe problem in calculating the flutter limit. One large contributor is on the stable and one large contributor on the unstable side of neutral. The aerodynamic damping is the small difference between these 2 large numbers. If one of the two changes only slightly, then the sum changes strongly and the sign may change.

## 5 MISTUNING EFFECTS ON AEROELASTIC STABILITY

In addition to normal tuned system aerodynamic damping calculations, also the effects of mistuning needs to be considered. The sources for mistuning are of random character given by the small stochastic variation of the blade geometry from manufacturing. In this case, a further aspect is the mistuning induced by the rapid pressure gauges and strain gauges that will be fitted onto the airfoils. In this section, an attempt is therefore made to quantify the stabilizing influence of mistuning on the rotor. The basis for the assessment is the choke flutter point from SIT's calculations ( $\Pi_{TT} = 1.38$  and 20,000 rpm), with a predicted minimum critical damping ratio of -0.23% in the tuned configuration.

The employed mistuned aeromechanical response model is an adaptation of the mistuning projection or subset of nominal modes (SNM) method proposed in [15,16]. The SNM approach is widely used thanks to its simplicity and computational efficiency, and it has been shown to be very accurate for small mistuning levels and negligible airfoil mode shape perturbations. This frequency domain method uses modal structural and aerodynamic coupling data in a traveling wave format, with projections of individual blade deviations (mass and/or stiffness-induced) along the elastic assembly modes. Moreover, the aerodynamic coupling is here implemented as complex stiffness contributions, which is considered valid within the small frequency range in question. In this case, the model covers the 1F mode family only, as it is well separated from higher modes. Hence, the mistuned response model consists of 21 degrees of freedom only.

In all cases considered, the analyses cover 10,000 randomly generated mistuned configurations (patterns), i.e., 10,000 random patterns are analyzed at each mistuning level. This investigation uses the simplest form of mistuning corresponding to uniform stiffness perturbations (Young's modulus variations). The random mistuning parameters are taken from truncated Gaussian distributions, implying that the infinite distribution "tails" are cut at

$\pm 3\sigma$ . The selection of a suitable frequency distribution from manufacturing tolerances etc. is by no means a clear-cut case, but a Gaussian distribution is usually the better choice according to experience versus a simple uniform distribution.

A convenient view of the mistuned system's stability behavior is given by figure 13, which shows the expected range of minimum damping found among the 10,000 patterns at each level of random frequency mistuning. The 0.1<sup>th</sup> percentile curve implies that there is a 0.1% "risk" that the minimum damping is below this curve. Conversely, the 99.9<sup>th</sup> and 90<sup>th</sup> percentile curves signify that there is a 0.1% (10%) risk that the minimum damping falls above the respective curve. The former (0.1<sup>th</sup> percentile) would normally be the curve to worry about during design, but here, of course, we are instead worried about turning stable.

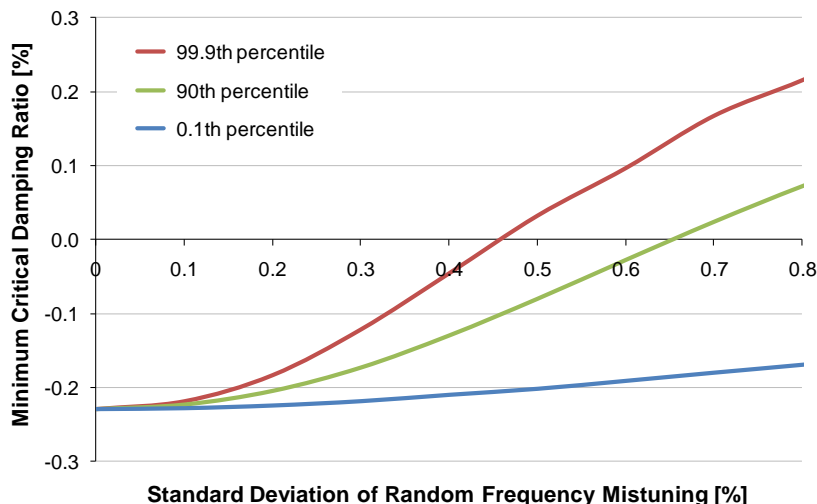


Figure 13: Blik aeroelastic stabilization characteristics with respect to random frequency mistuning. Displayed results are based on SIT data at  $\prod_{TT} = 1.38$  and 20,000 rpm.

It can be observed in figure 13 that the rate of stabilization is not linear with mistuning strength. Obviously, small levels of mistuning are not sufficient to overcome the relatively strong aerodynamic coupling in this case and to cause a significant break-up of symmetry. The latter implies participation of additional nodal diameter modes, which constitutes the mechanism behind increases in aerodynamic damping. This circumstance also becomes evident in figure 14. This shows, for each level of random frequency mistuning, the nodal diameter contents in the least stable mode of the mistuned configuration that corresponds to the 99.9<sup>th</sup> percentile. Hence, the aerodynamic damping associated with the modes shown in figure 14 form the 99.9<sup>th</sup> percentile curve in figure 13. The tuned case in the back end of the plot obviously consists only of forward traveling wave motion with three nodal diameters. As small levels of mistuning are introduced, the system responds immediately with the three nodal diameter symmetry breaking up into several participating nodal diameters. However, the dominance of the unstable forward three nodal diameter motion clearly remains up to about 0.3-0.4% frequency mistuning standard deviation. Above this level, the three nodal diameter motion has deteriorated into significant participation of several surrounding nodal diameters.

Reverting back to figure 13, it can be observed that beyond the initial nonlinear regime up to the aforementioned 0.3-0.4% frequency mistuning standard deviation level, the system's response to mistuning becomes essentially linear within the depicted range of mistuning levels. The rate of stabilization in this linear regime is approximately 0.07% of the critical

damping ratio per 0.1% increase in frequency mistuning standard deviation for the 99.9<sup>th</sup> percentile. The corresponding rate for the 90<sup>th</sup> percentile is 0.05%. Overall, the depicted stabilization behavior with mistuning is consistent qualitatively as well as quantitatively with prior SIT numerical investigations of transonic compressor blades in choke flutter, when differences in blade-to-blade coupling and damping magnitudes are accounted for [17].

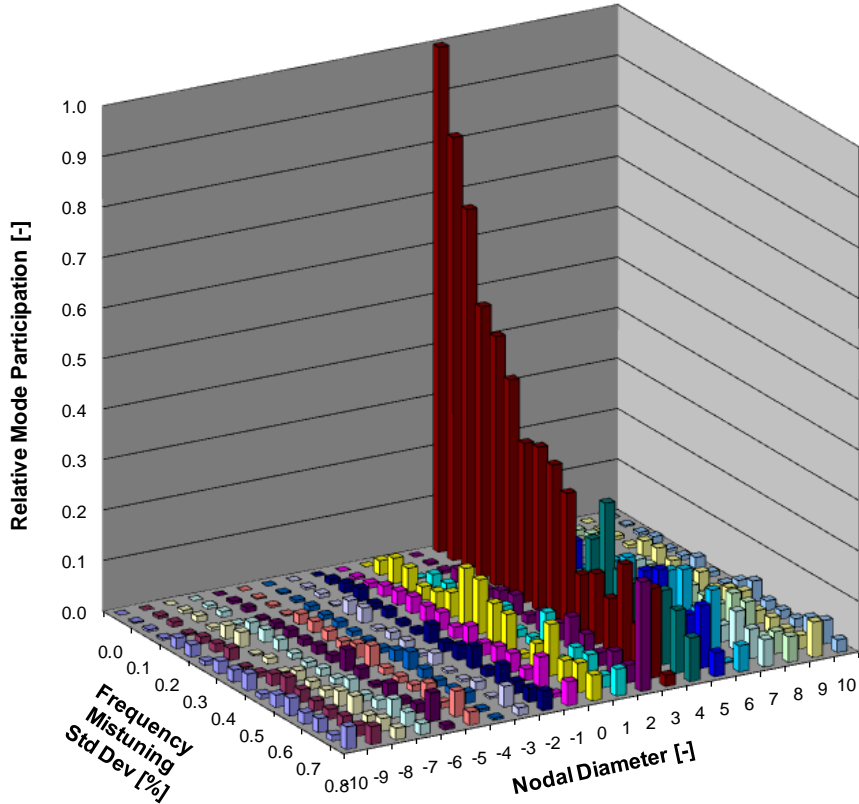


Figure 14: Participation of nodal diameters in the least stable mode of the mistuned configuration corresponding to the 99.9<sup>th</sup> percentile for increasing levels of random frequency mistuning. Displayed results are based on SIT data at  $\Pi_{TT} = 1.38$  and 20,000 rpm.

With the present goal of achieving flutter, the range of acceptable random mistuning levels, e.g., from manufacturing, is determined by the point where the 99.9<sup>th</sup> or 90<sup>th</sup> percentile (depending on accepted risk) reaches a critical damping level that allows for mechanical damping and overall uncertainties in the system. Current experience of typical blisk mistuning levels is that the standard deviation of random frequency mistuning of the 1F mode is less than 0.5%. From the current analysis this gives that the critical damping ratio for the 90<sup>th</sup> percentile is expected to be less than -0.08%. Clearly, there are great uncertainties in predicted aerodynamic damping levels and dissipative properties of instrumentation. However, helped by the strong blade-to-blade aerodynamic coupling, the present mistuning assessment shows that the rotor should respond with fairly distinct traveling wave motion and thus retain instability for typical levels of mistuning.

## 6 CONCLUSIONS

With respect to the analysis methods and predictions the quantitative differences in results for the computations are striking. Although for design purposes this is built into the criteria and design logic used at the companies for design, the need is clear for a more quantitative basis for the comparison. It has also been shown that large variations in where the aerodynamic damping becomes negative must be expected. Although large similarities in the predictions can be identified with respect to operating conditions the sensitivity of identifying the flutter limit itself quantitatively remains challenging, as small off-sets can cause a sign change in the critical (minimum damped) mode. Also noted are narrow regions, where the aerodynamic damping changes rapidly with flow condition such as towards the stall line. With the presented design and the following testing and analyses that are conducted in the program the understanding of the phenomena and how to analyze flutter in compressor design will improve.

The mistuning assessment shows that the strong blade-to-blade aerodynamic coupling in the test configuration leads to fairly distinct traveling wave motion for achievable low levels of mistuning. Nevertheless, the stabilizing effect of rotor mistuning due manufacturing tolerances and instrumentation is not negligible. It is therefore important to make every effort to minimize mistuning during instrumentation installation.

A test object has been designed where a large range of conditions can be tested and details measured. This increases the possibilities of improving the quantitative comparisons between test and computation, and thereby to develop more accurate prediction techniques.

## 7 REFERENCES

- [1] Holzinger F., Biela C., Schiffer H-P, Östlund J. Mårtensson H., " *Development of an Excitation System For Forced Response Investigation in the TU Darmstadt Compressor*", 12th International Symposium of Unsteady Aerodynamics, Aeroacoustics & Aeroelasticity of Turbomachines, 2009, ISUAAAT- I12-S3-4
- [2] Dhondt Guido. *The Finite Element Method for Three-dimensional Thermomechanical Applications*. Munich, Germany. 2004, ISBN 0-470-85752-8 John Wiley & Sons Ltd.
- [3] Lindström D., Mårtensson H., " *A method for flutter calculations based on the linearised compressible Euler equations*", IFASD 64, 2001
- [4] Baldwin, B. S., and Lomax, H., 1978. " *Thin Layer Approximation and Algebraic Model for Separated Turbulent Flows*". AIAA Paper No. 78-0257.
- [5] Ning, W., and He, L., 1998. " *Computation of Unsteady Flows Around Oscillating Blades Using Linear and Nonlinear Harmonic Euler Methods*". Journal of Turbomachinery, **120**(3), pp. 508–514.
- [6] He, L., 2000. " *Three-Dimensional Unsteady Navier-Stokes Analysis of Stator-Rotor Interaction in Axial-Flow Turbines*". Journal Proceedings of the Institution of Mechanical Engineers, Part A: Journal of Power and Energy, **214**(1), pp. 13–22.
- [7] Chen, T., Vasanthakumar, P., and He, L., 2001. " *Analysis of Unsteady Bladerow Interaction Using Nonlinear Harmonic Approach*". Journal of Power and Propulsion, **17**(3), pp. 651–658.
- [8] Eulitz, F., Engel, K., Nuernberger, D., Schmitt, S., Yamamoto, K.: " *On Recent Advances of a Parallel Time-Accurate Navier-Stokes Solver for Unsteady Turbomachinery Flow*",

Proceedings of the 4<sup>th</sup> ECCOMAS, Papailiou et al., eds., John Wiley & Sons, Vol. 1, pp. 252-258, 1998.

- [9] Nuernberger, D., Eulitz, F., Schmitt, S., Zachcial, A.: “*Recent Progress in the Numerical Simulation of Unsteady Viscous Multistage Turbomachinery Flow*”, ISABE-2001-1081, 2001.
- [10] Kahl, G.: “*Application of the time linearized euler method to flutter and forced response calculations*”, ASME-paper 95-GT-123, Houston, Texas, June 5-8, 1995
- [11] Kahl, G.; Klose, A.: “*Computation of time linearized transonic flow in oscillating cascades*”, ASME-paper 93-GT-269, Cincinnati, Ohio, May 24-27, 1993
- [12] Kahl G. *Aeroelastic Effects of Mistuning and Coupling in Turbomachinery Bladings*. PhD thesis, EPF Lausanne, Switzerland, 2002.
- [13] Mårtensson H., Vogt D., Fransson T., “*Assessment of a 3D linear Euler flutter prediction tool using sector cascade data*”, Proceedings of ASME Turbo Expo 2005, June 6-9, 2005, Reno-Tahoe, Nevada, USA
- [14] Carta F.O. “*Coupled Blade-Disk-Shroud Flutter Instabilities in Turbojet Engine*”. Journal of Engineering for Power, pages 419–426, July 1967.
- [15] Bladh, R., Castanier, M. P., and Pierre, C., 2001. “*Component-Mode-Based Reduced Order Modeling Techniques for Mistuned Bladed Disks—Part I: Theoretical Models*”. Journal of Engineering for Gas Turbines and Power, **123**(1), pp. 89–99.
- [16] Yang, M.-T., and Griffin, J. H., “*A Reduced Order Model of Mistuning Using a Subset of Nominal System Modes*,” Journal of Engineering for Gas Turbines and Power, Vol. 123, No. 4, 2001, pp. 893–900.
- [17] Zhai, Y., Bladh, R., and Dyverfeldt, G., 2011. “*Aeroelastic Stability Assessment of an Industrial Compressor Blade Including Mistuning Effects*”, ASME Paper no. GT2011-45800, Proceedings of ASME Turbo Expo 2011, Vancouver, Canada.